DOI: 10.1002/chem.201204296

VIP

Siamese-Twin Porphyrin: A Pyrazole-Based Expanded Porphyrin of Persistent Helical Conformation

Lina K. Blusch,[a] Yasmin Hemberger,[b] Kevin Pröpper,[a] Birger Dittrich,[a] Franziska Witterauf,[b] Michael John,[a] Gerhard Bringmann,*[b] Christian Brückner,*[c] and Franc Meyer*[a]

Abstract: The 3+3-type synthesis of a pyrazole-based expanded porphyrin **22H$_4$**, a hexaphyrin analogue named Siamese-twin porphyrin, and its homobimetallic diamagnetic nickel(II) and paramagnetic copper(II) complexes, **22Ni$_2$** and **22Cu$_2$**, are described. The structure of the macrocycle composed of four pyrroles and two pyrazoles all linked by single carbon atoms, can be interpreted as two conjoined porphyrin-like subunits, with the two opposing pyrazoles acting as the fusion points. Variable-temperature 1D and 2D NMR spectroscopic analyses suggested a conformationally flexible structure for **22H$_4$**. NMR and UV/Vis spectroscopic evidence as well as structural parameters proved the macrocycle to be non-aromatic, though each half of the molecule is fully conjugated. UV/Vis and NMR spectroscopic titrations of the free base macrocycle with acid showed it to be dibasic. In the complexes, each metal ion is coordinated in a square-planar fashion by a dianionic, porphyrin-like {N$_4$} binding pocket. The solid-state structures of the dication and both metal complexes were elucidated by single-crystal diffractometry. The conformations of the three structures are all similar to each other and strongly twisted, rendering the molecules chiral. The persistent helical twist in the protonated form of the free base and in both metal complexes permitted resolution of these enantiomeric helimers by HPLC on a chiral phase. The absolute stereostructures of **22H$_6^{2+}$**, **22Ni$_2$**, and **22Cu$_2$** were assigned by a combination of experimental electronic circular dichroism (ECD) investigations and quantum-chemical ECD calculations. The synthesis of the first member of this long-sought class of expanded porphyrin-like macrocycles lays the foundation for the study of the interactions of the metal centers within their bimetallic complexes.

Keywords: copper · chirality · nickel · pH titration · porphyrins · pyrazole

Introduction

Expanded porphyrins are higher analogues of porphyrins, that is, porphyrinoids with more ring atoms than a porphyrin. Since the time they were serendipitously discovered,[1] the field has become a multi-faceted area of research that has had broad impact on our understanding of fundamental issues such as anion binding[2] or aromaticity.[3] Hückel aromatic, anti-aromatic, non-aromatic, and Möbius aromatic expanded-porphyrin systems have been realized.[4] Also, a plethora of useful compounds were introduced, among them macrocycles with actinide coordination capabilities,[5] efficacy in the photodynamic therapy of tumors[6] or as MRI agents,[7] or compounds possessing pronounced non-linear optical properties.[8] Particularly the reports by the groups of Sessler, Osuka, Kim, Latos-Grazynski, and Chandrashekar over the past decade have lent distinction to the field.[9] A number of recent reports deal with the fusion of multiple porphyrins or porphyrin-like macrocycles into larger systems, the formation of their multi-metallic complexes, and the study of their physical properties.[10]

The conformational diversity among expanded porphyrins is vast because of their enormous structural variability: For instance, expanded porphyrins may contain pyrroles or other heterocycles (furans, thiophenes, etc.), the pyrrolic building blocks may be directly connected, linked by single atoms or multi-carbon chains (of varying hybridization), imine linkages may be present, and the pyrroles may be inverted or present in an N-confused fashion (2,4-linked rather than the traditional 2,5-linkage),[11] or coordinated metal ions can be present in the porphyrinoid centers.[12] In addition, the macrocycle conformation is controlled by tem-

[a] Dr. L. K. Blusch,[+] Dipl.-Chem. K. Pröpper, B. Dittrich, Dr. M. John, Prof. Dr. F. Meyer
Institute of Inorganic Chemistry, University of Göttingen
Tammannstr. 4, 37077 Göttingen (Germany)
Fax: (+49) 551-39-3063
E-mail: Franc.Meyer@chemie.uni-goettingen.de

[b] Dipl.-Chem. Y. Hemberger, Dipl.-Chem. F. Witterauf, Prof. Dr. Dr. h.c. mult. G. Bringmann
Institute of Organic Chemistry, University of Würzburg
Am Hubland, 97074 Würzburg (Germany)
E-mail: bringman@chemie.uni-wuerzburg.de

[c] Prof. Dr. C. Brückner
Department of Chemistry, University of Connecticut
Storrs, Connecticut 06269-3060 (USA)
E-mail: c.bruckner@uconn.edu

[+] née Frensch.

Supporting information for this article is available on the WWW under http://dx.doi.org/10.1002/chem.201204296.

perature, solvent, degree of oxidation, and/or protonation levels.[9a] The conformation of hexaphyrin **1**, one of the older and best-studied example of an expanded porphyrin, for instance,[13] is mainly planar, with two pyrroles inverted, but variation of the substitution pattern and/or oxidation state introduces dumbell-shaped or figure-eight conformations (Scheme 1).[9c] Free-base heptaphyrin **2**[14] and octaphyrin **3**[15] generally adopt figure-eight conformations.

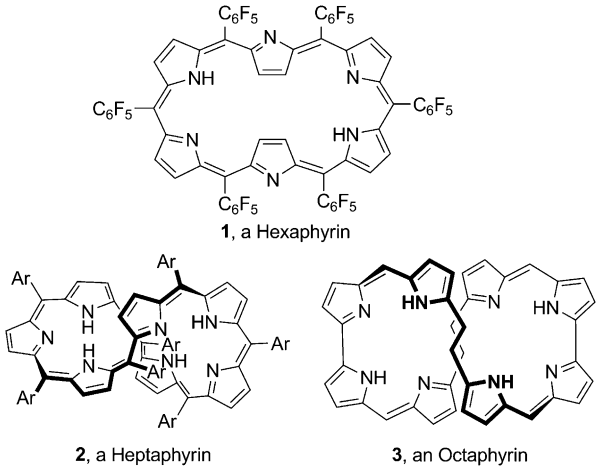

Scheme 1. Selected expanded porphyrins; β-substituents of octaphyrin omitted for clarity.

It is well-established that pyrazoles with chelating side-arms can act as bridging ligands in highly preorganized dinuclear transition metal complexes.[16] Such pyrazole-based chelates proved to be versatile and useful building blocks in bioinorganic coordination chemistry as they offer a good compromise for mimicking the bridging carboxylate donors frequently found in bimetallic enzymes in Nature and because they could be readily incorporated into compartmentalized ligand frameworks.[17] In these complexes, the pyrazoles are monoanionic donors supporting a range of metal–metal distances.[18]

The integration of pyrazole moieties (or other heterocycles such as imidazoles,[19] oxazoles,[20] thiadiazoles, or triazoles[21]) in porphyrinoid macrocyclic compounds is, however, little developed. Only one family of porphyrin analogues incorporating a pyrazole, carbaporphyrins **4**, recently introduced by the group of Lash, is known.[22] One other multidentate cyclic pyrazole–pyrrole hybrid ligand was reported, compound **5**,[23] but this macrocycle cannot be categorized as a true porphyrinoid, that is, containing a fully conjugated framework.

A formal replacement of the two inverted pyrroles in hexaphyrin by pyrazoles gives rise to the scaffold structure shown in Scheme 2. The resulting expanded porphyrin, consisting of four pyrroles and two pyrazoles, merges the structural characteristics of pyrazoles bearing chelating side-arms with those of porphyrins; it can also be interpreted as the fusion of two porphyrin-like coordination sites. We thus

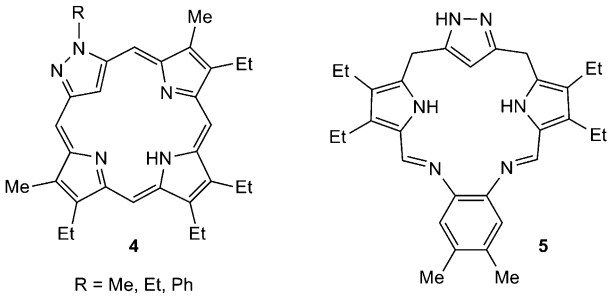

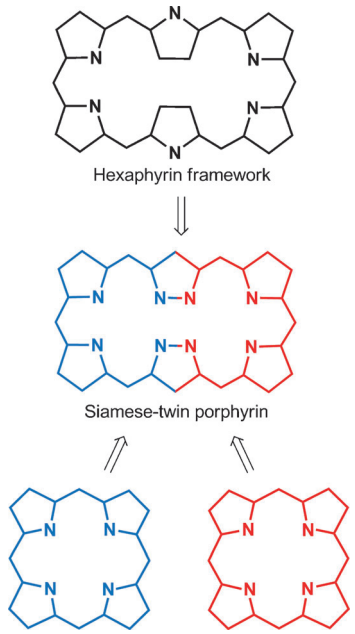

Scheme 2. The Siamese-twin porphyrin framework structure as derived from the hexaphyrin structure, simultaneously highlighting the fusion of two porphyrin-like halves of the molecule.

named it the "Siamese-twin porphyrin".[24] This naming is descriptive of the framework structure but shall not evoke any implications about the presence of aromatic conjugation pathways. One of the goals of this target structure was to incorporate two metal ions in these highly preorganized binding pockets in close proximity to each other and to study the resulting metal–metal cooperativity.

We are not the first to conceive the twin-porphyrin framework structure. Lind, in a 1987 dissertation,[25] described several approaches towards this expanded porphyrin. Invariably, however, they were unsuccessful. With the benefits of hindsight, this can be attributed to a number of factors: The key intermediate for the 3+3-MacDonald-type strategies pursued was a pyrazole analogue to a tripyrrane, bispyrrolylpyrazole **10** (Scheme 3). It was synthesized by the acylation of dimethylpyrrole **8** by the activated pyrazole diester **7**, itself obtained from well-known pyrazole diester **6**. Reduction of bisketone **9** generated compound **10**. However, its synthesis succeeded only as the pyrazole-*N*-substituted de-

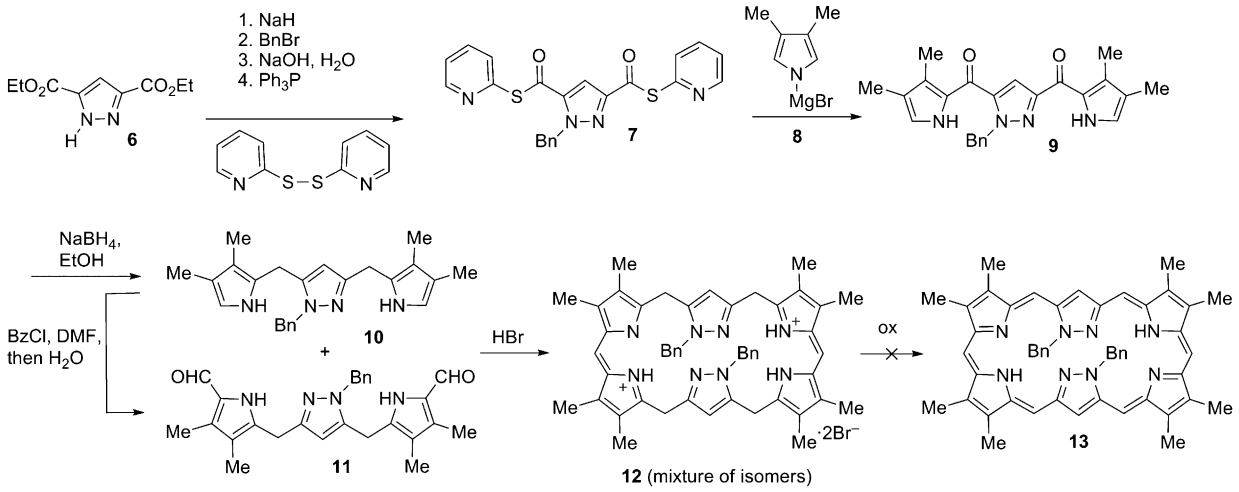

Scheme 3. Lind's attempted synthesis of the twin porphyrin **13**.

rivative. Whereas **10** could be successfully diformylated to provide **11**, and the 3+3 condensation of **10** and **11** led to macrocycle **12**, the pyrazole benzyl protection group (Bn) could not be removed. This, however, may have been the crucial factor in Lind's inability to convert framework **12** to the fully conjugated (planar) twin-porphyrin framework structure **13**. Particularly problematic was the oxidation of the pyrrole–pyrazole bridging *meso*-carbon atoms.

When we embarked on the synthesis of the twin-porphyrin framework, we also decided to pursue a 3+3 strategy similar to Lind's. Based on our experience with the functionalization of pyrroles and pyrazoles, we devised an alternative strategy towards the assembly of the key building block, bis(pyrrolyl-methylene)-pyrazoles **14**, which was based on an alkylation of an α-unsubstituted pyrrole with a pyrazole.[23] We thus directly delivered sp^3-linkages between the pyrazole and pyrroles. A double Vilsmeyer–Haak formylation of **14** generated bisaldehydes **15**. This strategy requires fewer steps than Lind's synthesis of the equivalent building block, but most importantly, it avoids the use of a pyrazole protecting group.

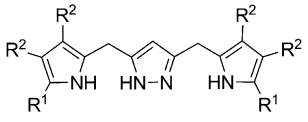

14a, R^1 = H, R^2 = H
14b, R^1 = H, R^2 = Et
15a, R^1 = CHO, R^2 = Et
15b, R^1 = CHO, R^2 = Et

Unfortunately, the 3+3-type syntheses of the target macrocycles could not be achieved at the time, though other interesting, non-conjugated macrocycles, such as **5**, were prepared and studied.[23] Three major obstacles became evident in our work, some of which mirrored the problems in Lind's work: Whereas mass spectrometry (MS) indicated that a 3+3 macrocyclization of the pyrrolyl–pyrazole building blocks had likely taken place, their conformational flexibility and the large number of stereoisomers formed posed great technical difficulties. As a result, the macrocycles could not be isolated or spectroscopically unambiguously characterized. Even more damaging, our inability to reliably oxidize any sp^3-carbon atoms attached to the pyrazoles hampered any progress. Thus, even though we avoided the need of pyrazole protecting groups, we still faced the same oxidation problem that Lind described. Notably, Lash et al. also described their difficulties in oxidizing the equivalent positions in their attempts to synthesize carbaporphyrin **4**, thus pointing to a general problem when incorporating pyrazoles into porphyrinoids.[22]

Guided by these experiences, our renewed efforts were finally successful and the twin porphyrin and its homobimetallic $\mathbf{22Cu_2}$ complex were described in a preliminary report.[24] Following up on this, we provide here the details of the design and synthesis of the free-base twin porphyrin $\mathbf{22H_4}$ and the formation and structure of its dicopper(II) complex $\mathbf{22Cu_2}$. Furthermore, we will firstly report the synthesis and crystal structure of the homobimetallic diamagnetic dinickel(II) complex $\mathbf{22Ni_2}$, as well as the crystal structure of the protonated form of free-base twin porphyrin $\mathbf{22H_6}^{2+}$, revealing the highly twisted chiral conformations already observed for the dicopper complex.[24] A series of NMR and UV/Vis spectroscopic investigations allowed conclusions to be drawn on the protonation- and temperature-dependent conformational characteristics of the macrocycles and the prevailing conjugation pathways. Importantly, the helimeric conformations of the macrocycles were found to be persistent. We will thus also describe the resolution of the enantiomers by HPLC on a chiral phase and the investigation of the respective helical stereoisomers by online LC-ECD measurements. A comparison of their experimental ECD spectra with the quantum-chemically calculated ones permitted assignment of their absolute stereostructures.

Results and Discussion

Synthesis of the twin porphyrin $22H_4$: We hypothesized that the substitution of all *meso*-positions with phenyl groups would facilitate the oxidation of the macrocycle by offering additional conjugation. We further assumed that the decoration of all β-positions of the pyrroles and the pyrazole β-carbon atoms would enforce a conformation of the macrocyclic, non-conjugated precursor that places all substituents on the outside, further facilitating its oxidation and formation of the target structure. Indeed, this strategy proved to be successful (Scheme 4).

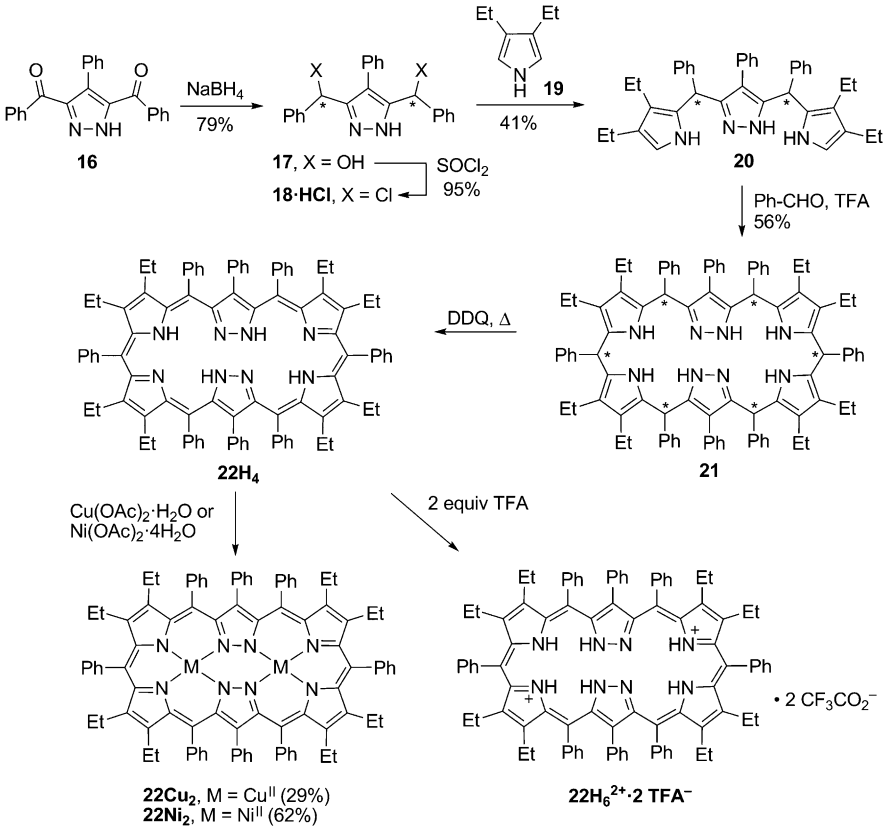

Scheme 4. Synthesis of the twin porphyrin $22H_4$ and its homobimetallic complexes.

The key building block in the 3+3 synthesis of $22H_4$ is the all-β- and *meso*-substituted pyrrole–pyrazole hybrid **20**. Its synthesis started from our previously reported precursor 3,5-dibenzoyl-4-phenyl-1*H*-pyrazole (**16**).[26] The reaction series (reduction to give **17**, followed by halogenation to provide **18** and subsequent substitution with 3,4-diethylpyrrole **19** to form compound **20**) was modeled after the synthesis of the pyrrole–pyrazole hybrid **14** reported by us earlier.[23a] This pyrazole analogue of a tripyrrane was isolated as a mixture of stereoisomers. The spectroscopic signatures of **20** confirmed its connectivity. The acid-catalyzed 3+3-type condensation of two equivalents of the pyrrole–pyrazole hybrid **20** with two equivalents of benzaldehyde proceeded smoothly, providing **21**. This compound, an all-sp^3-linked macrocycle, was isolated as a mixture of stereoisomers (as indicated by the presence of multiple peaks for its diagnostic signals in the NMR spectra). Similarly to the octa-β-alkyl, *meso*-tetraarylporphyrinogen, the steric hindrance between the *meso*- and the β-substituents stabilizes this leuco compound against rapid aerial oxidation.[27] However, heating the light-yellow solution of **21** with four equivalents of DDQ in toluene for 12 min resulted in the formation of a deep-green solution. This reaction time should not be exceeded to minimize decomposition reactions. Column chromatography on silica gel with *n*-hexane and ethyl acetate (in a 2:1 ratio) provided the green product $22H_4$ as the first major fraction. Evaporation of the solvent and taking up the crude green solid in a minimal amount of acetone, and subsequent solvent removal of the filtrate provided spectroscopically pure $22H_4$. The HR-MS ($m/z = 1301.6895$) data suggested a composition of $C_{92}H_{85}N_8$ (for $[MH^+]$), as expected for the (monoprotonated) target free-base twin porphyrin $22H_4$.

UV/Vis spectroscopic properties of twin porphyrin $22H_4$ in its neutral, mono-, and diprotonated states: The UV/Vis spectrum of the neutral macrocycle $22H_4$ shows two relatively broad main absorption bands at 390 and 639 nm in a ≈2:1 ratio (plus a shoulder at 734 nm). The bands are characterized by extinction coefficients of, or under, $10^5\,L\,mol^{-1}\,cm^{-1}$ (Figure 1, Table 1). In comparison, porphyrins exhibit extinction coefficients for their Soret bands that are frequently higher.[28] Thus, the spectrum resembled much more those of linear oligopyrrolic pigments,[29] indicating the presence of extensive conjugation but not of an aromatic porphyrin-like π-system. A UV/Vis titration of $22H_4$ with trifluoroacetic acid (TFA) in CH_2Cl_2 allowed the characterization of the macrocycle as dibasic. Upon protonation, only a subtle color change was observed (Figure 1). Addition of one equivalent of TFA caused only a minor intensity increase and redshift of the long-wavelength shoulder (to 753 nm), whereas the intensity of the band at 390 nm decreased only a little. Addition of a second equivalent of TFA resulted in a slight shift of the band at 390 nm (to 400 nm) but the band at 639 nm increased to ≈80% of the intensity of the high-energy band. No further changes were observed beyond the addition of two equivalents of acid. This spectral behavior upon proto-

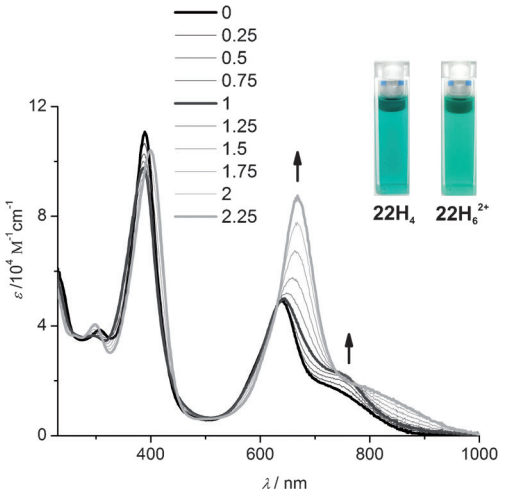

Figure 1. UV/Vis spectroscopic titration of **22H$_4$** in CH_2Cl_2 with 0 to 2.25 equivalents of TFA.

Table 1. UV/Vis spectral data of the compounds **22H$_4$**, **22H$_6^{2+}$**, **22Ni$_2$**, and **22Cu$_2$**.

λ/nm (ε /10^4 L mol^{-1} cm^{-1})			
22H$_4$	**22H$_6^{2+}$**	**22Ni$_2$**	**22Cu$_2$**
390 (11)	400 (10)	377 (6.2)	391 (4.6)
639 (4.9)	668 (8.7)	547 (2.6)	629 (2.2)
734 (1.7)	795 (1.8)	765 (1.4)	

nation is untypical of π-aromatic porphyrinoid macrocycles but is reminiscent of bilindiones and related linear oligopyrrolic pigments.[29]

NMR spectroscopic characterization of free-base twin porphyrin 22H$_4$: The ^{1}H NMR spectrum of **22H$_4$** in CD_2Cl_2 at ambient temperature is broadened and of marginal diagnostic value (Figure 2). Apart from the presence of signal clusters assigned to the phenyl and the ethyl substituents, not much more can be interpreted. Cooling to 248 K significantly sharpened the peaks, indicating that much of the signal broadening can be attributed to dynamic processes. At this temperature, macrocycle **22H$_4$** exhibited more signals assigned to methylene protons than the two signals anticipated for the highly symmetric constitution of the twin porphyrin (or four signals if NH tautomerism was slow). Also, the CH_3 protons appeared as four distinct triplets (see the also low-temperature ^{1}H^{1}H-COSY spectrum in the Supporting Information, Figure S2). This indicated the presence of a structural property that reduces the overall symmetry of the macrocycle. Vogel and co-workers observed the diastereotopic splitting of the methylene protons for **3** as a consequence of its twisted geometry.[30] In the case of **22H$_4$**, the appearance of the diastereotopic methylene signals can also be rationalized by assuming that a similar conformational effect leads to the formation of a chiral molecule. This assumption was confirmed by single-crystal diffractometry (see below).

One other diagnostic feature in the ^{1}H NMR spectrum of **22H$_4$** at 248 K was the presence of low-field signals (at $\delta =$ 11.38 and 13.34 ppm) assigned to the inner NH protons. As expected, these protons were readily exchanged with [D$_4$]MeOD. The low-field chemical shifts of the NH protons were a clear indication for the absence of any macrocyclic diatropic ring current induced by a macrocyclic π-aromatic system that would have shifted the signals significantly below $\delta = 1$ ppm. Alternatively, low-field-shifted pyrrole and pyrazole NH signals may be attributed to the presentation of the NH groups pointing towards the outside of an aromatic macrocycle. However, NOESY experiments showed a correlation of the NH signals with each other (the Supporting Information, Figure S5), indicating that they are all oriented inwards. Thus, NMR spectroscopy provided evidence that the presence of the β- and *meso*-substituents had the desired conformational consequences.

The presence of two distinct, relatively sharp NH signals of equal intensity in the ^{1}H NMR spectrum of **22H$_4$** at 248 K again indicated an overall two-fold symmetry of the free base in solution (Figures 2 and 3). The diagnostic NH ^1J coupling constants observed in the ^{1}H^{15}N-HMBC NMR spectrum of **22H$_4$** permitted an assignment of the two signals (Figure 4; for a more detailed discussion of this spectrum, see below).[31] The signal at $\delta = 11.38$ ppm was attributed to the pyrrole NH proton (N^{pyr} at $\delta = -244$ ppm; $^1J(NH) = 95$ Hz) and the signal at $\delta = 13.34$ ppm to the pyrazole NH (N^{pz} at $\delta = -168$ ppm; $^1J(NH) = 107$ Hz).

Protonation of 22H$_4$ and its analysis by using NMR spectroscopy: The structure of **22H$_4$** implied the presence of two

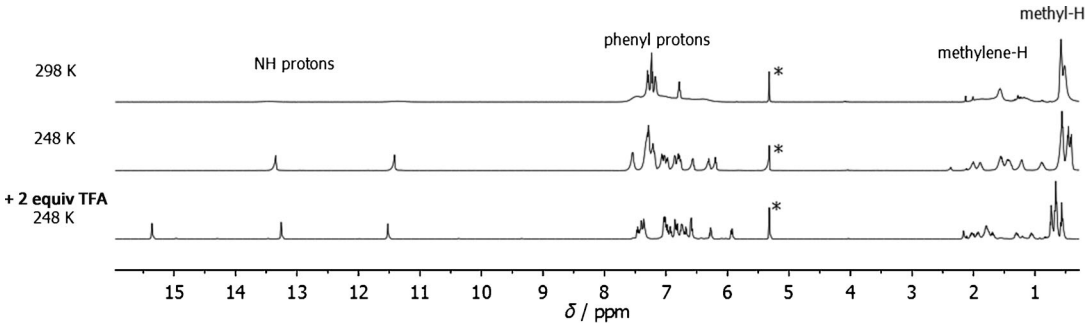

Figure 2. ^{1}H NMR spectrum (500 MHz, CD_2Cl_2) of **22H$_4$** under the indicated conditions. The residual solvent signal is marked with an asterisk (*).

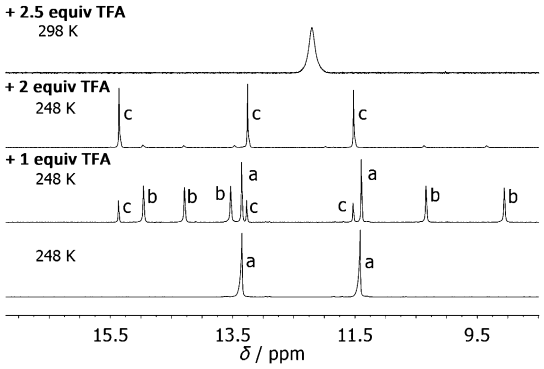

Figure 3. Downfield region of the ^{1}H NMR spectrum (500 MHz, CD_2Cl_2, 248 K) highlighting the changes assigned to the NH proton signals upon stepwise protonation (cf. also to Figure S4, the Supporting Information). Signal set a was assigned to **22H$_4$**, signal set b to **22H$_5^+$**, and signal set c to **22H$_6^{2+}$**.

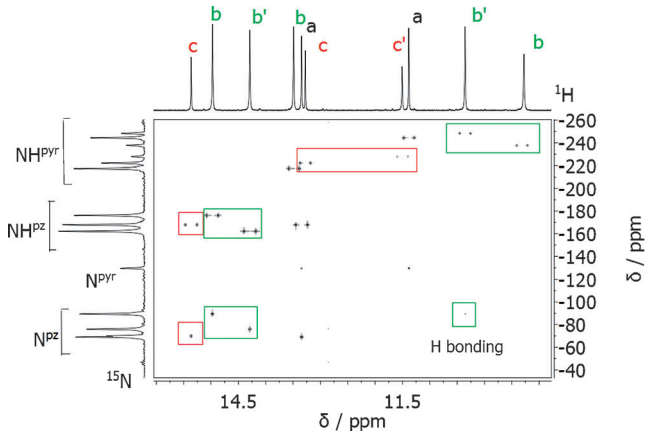

Figure 4. ^{1}H^{15}N-HMBC spectrum (500 MHz, CD_2Cl_2, 243 K) of **22H$_4$**+1 equivalent TFA. A mixture of three differently protonated species is present: **22H$_4$** (a), **22H$_5^+$** (b and b′) and **22H$_6^{2+}$** (c and c′).

basic imine-type pyrroles and two significantly less-basic pyrazole imine nitrogens. Protonation studies confirmed this. NMR titrations of **22H$_4$** with TFA were performed, showing diagnostic changes (Figure 3). Particularly the low-field region of the spectra warranted a closer inspection as they permitted conclusions to be drawn on the protonation site and the existence of distinct mono- and diprotonated species. Addition of a single equivalent of TFA generated a number of additional signals. Next to a substantial portion of unaltered **22H$_4$** (indicated species a), two more species (b and c) became apparent. Upon addition of the second equivalent of TFA, species c became the major product and only traces of b remained. Thus, the higher-symmetry species c is the diprotonated molecule **22H$_6^{2+}$** and, consequently, species b can be assigned as the low-symmetry monoprotonated species **22H$_5^+$** carrying five non-equivalent NH protons (Scheme 5).

The existence of a temperature-dependent equilibrium between the neutral, monoprotonated, and diprotonated species in the presence of a single equivalent of protons (equilibrium shifted towards the monoprotonated species at lower

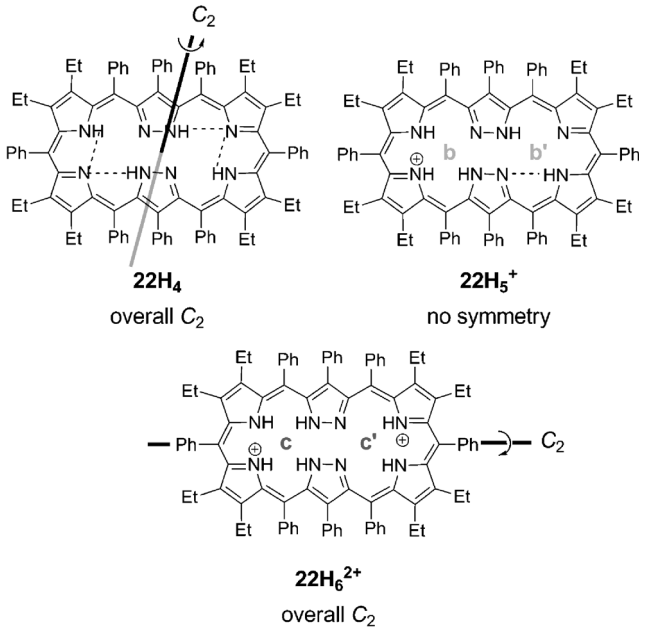

Scheme 5. Spectroscopically derived structures and H-bond patterns in the three protonation states of **22H$_4$**.

temperatures) implied that the basicity of the free base a, monoprotonated species b, and diprotonated species c are relatively close to each other. This indicated the presence of two essentially independent electronic systems. In case of a strong electronic coupling (through, for instance, conjugation), one would have expected the basicity of the monoprotonated species to be much more reduced compared with that of the neutral species, such that no significant quantities of the diprotonated species would have been formed before the vast majority of the neutral species would have been monoprotonated.

A ^{1}H^{15}N-HMBC spectrum of the mixture of the three species, **22H$_4$** (a), **22H$_5^+$** (b) and **22H$_6^{2+}$** (c) after the addition of one equivalent of TFA was recorded at 243 K (Figure 4). This, and the NOESY spectroscopy (the Supporting Information, Figure S5), also allowed us the assignment of the location of the protons and the resulting intramolecular H-bond pattern (Scheme 5). As predicted, based on the general basicity of the pyrrolic imine nitrogens and pyrazoles, the protons were found to be located on the pyrrole imine nitrogens, and each half of the molecule to be sequentially monoprotonated. ^{13}C NMR spectra also confirmed these assignments based on the symmetry elements visible (the Supporting Information, Figures S3 and S7). Addition of an excess of TFA led to a fast scrambling of all pyrazole protons and the number of signals was reduced to one quarter (the Supporting Information, Figures S8–S10).

Besides the ^1J couplings, ^2J interactions for the H–N^{pz}–N^{pz} hydrogens were also detectable in the ^{1}H^{15}N-HMBC spectrum (Figure 4). Further, cross-peaks provided evidence for the presence of H-bonds between the NH^{pz} and NH^{pyr} protons to the neighboring imine-type N$^{pyr/pz}$ atoms, thus fully defining the H-bond patterns within the macrocycle

(Scheme 5). Somewhat surprisingly, macrocycle $\mathbf{22H_6}^{2+}$ features four protons in one $\{N_4\}$ compartment, but only two in the other $\{N_4\}$ compartment.

Solid-state conformation of the twin porphyrin $\mathbf{22H_6}^{2+}$: Crystals suitable for investigation by single crystal X-ray diffraction of $\mathbf{22H_6}^{2+}\cdot 2TFA^-\cdot x(CH_3)_2CO$ were obtained by slow solvent evaporation from a saturated solution of the macrocycle in acetone and TFA. The compound crystallized in the non-chiral space group *P*1 (with about 800 atoms per asymmetric unit; for further details see the Supporting Information). The resolution of the diffraction data did not provide decisive evidence of the protonation state of each relevant site in the macrocycle. However, UV/Vis and NMR spectroscopic solution-state investigations confirmed it to be present as a dication under the crystallization conditions. Hence this diprotonated species is likely also present in the crystal as well.

The molecular structure confirmed the connectivity of the free-base twin porphyrin structure (Figure 5A). The chromophore bond lengths showed an alternating short-long pattern (Figure 5B), providing further evidence for the presence of two essentially independent π-conjugation pathways that are each restricted to their half of the macrocycle (Figure 5C), thus excluding the presence of a 26-π system analogous to that found in hexaphyrins. While the pyrazoles represent the fusion points of two porphyrin-like $\{N_4\}$ chelation pockets, they also insulate the two π-systems from cross-talk with each other. In fact, the replacement of a pyrrolic building block in a porphyrin by a pyrazole in compound **4** also inhibits the aromatic conjugation pathway.[22a]

Importantly, the crystal structure demonstrates that the conformation of the macrocycle is severely twisted, mirroring the solution-state data. The helical twist along the long axis of the molecule (the *meso*$^{pyr/pyr}$ to *meso*$^{pyr/pyr}$ axis) renders it chiral. Given the non-chiral space group, the crystals of $\mathbf{22H_6}^{2+}$ must therefore be a racemic mixture of the *P*- and *M*-helimers. The helimer torsion angle τ (defined in Figure 5D as the α-C^{pyr}–*meso*-C$^{pyr/pyr}$–*meso*-C$^{pyr/pyr}$–α-C^{pyr} torsion angle) is approximately ±86°; the angle between the two N_4 mean planes is ≈41°.

The origin of the non-planarity of twin porphyrins $\mathbf{22H_4}$ and $\mathbf{22H_6}^{2+}$: Solution and solid-state investigations of the free base in neutral and protonated forms showed that the macrocycle adopts a drastically non-planar conformation. However, a DFT molecular model[32] of the macrocycle in the absence of any peripheral substituents suggests the macrocycle to be perfectly planar (Figure 6). Once the substituents were introduced or the macrocycle was diprotonated, the computations revealed non-planar conformations (see Supporting Information, Figure S20).

The conformational plasticity of porphyrinoids is well-known.[9c,d] Which particular conformation is favored depends on several factors, including intrinsic structural constraints, intramolecular hydrogen-bonding, the aromatic or anti-aromatic character of the conjugated π-system, and the presence and nature of peripheral substituents. In particular, [26]hexaphyrins were observed to assume a non-planar conformation upon introduction of bulky substituents.[33] This behavior is also observed in "regular" porphyrins. For instance, β-octaalkyl-*meso*-tetrakisaryl-substituted porphyrins are non-planar, whereas porphyrins with either β-octaalkyl- or *meso*-tetrakisaryl-substitution are relatively planar.[34] The computations of our twin porphyrin suggest that the introduction of only β-ethyl groups does not cause any distortion, but as soon as the *meso*-phenyl groups are introduced, it causes steric interactions that force the mac-

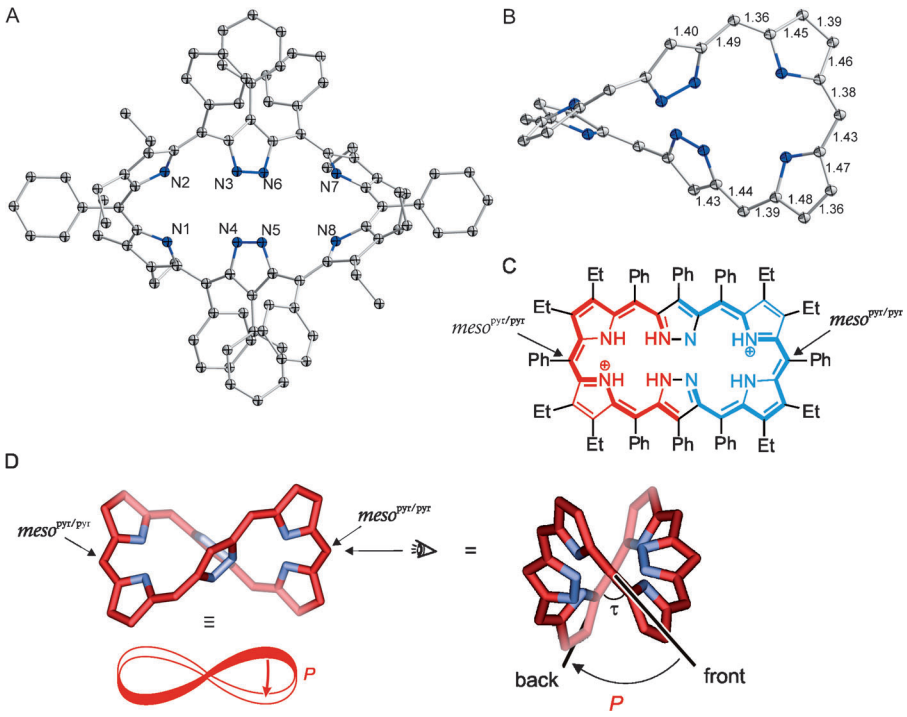

Figure 5. Molecular solid-state structure of $\mathbf{22H_6}^{2+}$: A) front view and labeling of atoms. B) side view and selected bond lengths in Å. Structure of $\mathbf{22H_6}^{2+}$ (C) in which the two independent π-conjugation pathways are highlighted and the *meso*$^{pyr/pyr}$ positions are marked. D) schematic representation of the *P*-enantiomer, the nomenclature of these helimers and the view along both *meso*$^{pyr/pyr}$ carbon atoms (long axis of the molecule) of the framework of $\mathbf{22H_6}^{2+}$, highlighting the torsion angle τ. All hydrogen atoms and residual solvent molecules were omitted for clarity, as were the phenyl and ethyl groups in B and D. In the solid-state structures arbitrarily, only the *P*-helical enantiomers are shown.

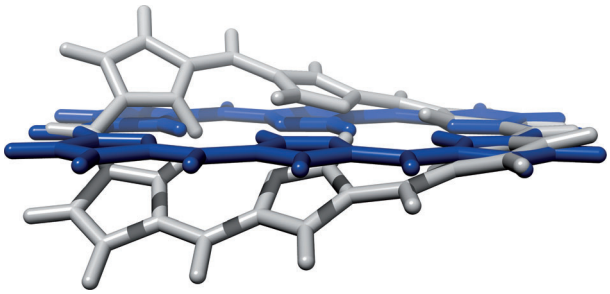

Figure 6. Molecular model (DFT, BP86 level)[32] of the twin-porphyrin framework in the absence of any substituents: free base (blue) and its protonated dicationic form (gray).

rocycle into a non-planar, twisted conformation (the Supporting Information, Figure S20). Experiments directed at relieving the steric congestion within the twin porphyrin framework are in progress.

Chiral resolution of the diprotonated species $22H_6^{2+}$ by using HPLC on a chiral stationary phase and assignment of the absolute stereostructures: Figure-eight and twisted conformations of expanded porphyrins are intrinsically chiral but in most cases the two helical enantiomers interconvert rapidly. However, Vogel et al. showed that β-hexadecaethyloctaphyrin **3** is conformationally stable enough to allow the separation of the two enantiomers by HPLC on a chiral stationary phase.[30] Osuka et al. also demonstrated the chiral resolution of a quadruply N-fused heptaphyrin.[35] Smaller porphyrinoids assuming stable twisted conformations were also chirally resolved.[36]

Attempts to separate any enantiomers of the neutral macrocycle $\mathbf{22H_4}$ failed but the HPLC separation of a racemic mixture of $\mathbf{22H_6}^{2+}$ on a chiral phase (Chiralpak IA column) succeeded in the presence of TFA (0.05% in ethyl acetate). Even though the retention times of the two stereoisomers (*P*-$\mathbf{22H_6}^{2+}$ and *M*-$\mathbf{22H_6}^{2+}$) were so similar to each other that, according to its HPLC-UV/Vis spectral trace, no resolution had taken place, HPLC-ECD showed a good resolution (see later, Figure 9), demonstrating once more the advantages of this technique.[37]

By using NOESY, a minimum level for racemization enthalpies $\Delta G^{\neq} = 100\ \mathrm{kJ\,mol^{-1}}$ for $\mathbf{22H_4}$ and of $105\ \mathrm{kJ\,mol^{-1}}$ for $\mathbf{22H_6}^{2+}$ could be estimated with the assumption of temperature-independent $\Delta G^{\neq}$ (details in the Supporting Information). Lifetimes were projected to be 12 h and 4 d, respectively. Thus, even though the diprotonated macrocycle is slighty more stable, the inability to separate the enantiomers of $\mathbf{22H_4}$ points to a separation problem rather than a fast enantiomeric interconversion considering the timescale of the resolution experiment.

A lack of precedents precluded an empirical assignment of the absolute stereostructure of the helical enantiomers of $\mathbf{22H_6}^{2+}$. We therefore determined their absolute configuration by quantum-chemical calculation of the CD spectra and comparison with the experimental ones.[38] This approach was already proven successful for the assignment of the absolute configurations of other chiral porphyrinoid systems with all kinds of stereogenic elements such as axes,[39] centers, and helices.[36] All calculations were performed by using the Gaussian 09 software package.[40] During the investigation of the conformational space of $\mathbf{22H_6}^{2+}$ by the B3LYP/6-31G(d,p)[41] method, we discovered that only two strain-free conformations of the backbone existed, each with all possible combinations of the different orientations of the ethyl substituents (Figure 7).

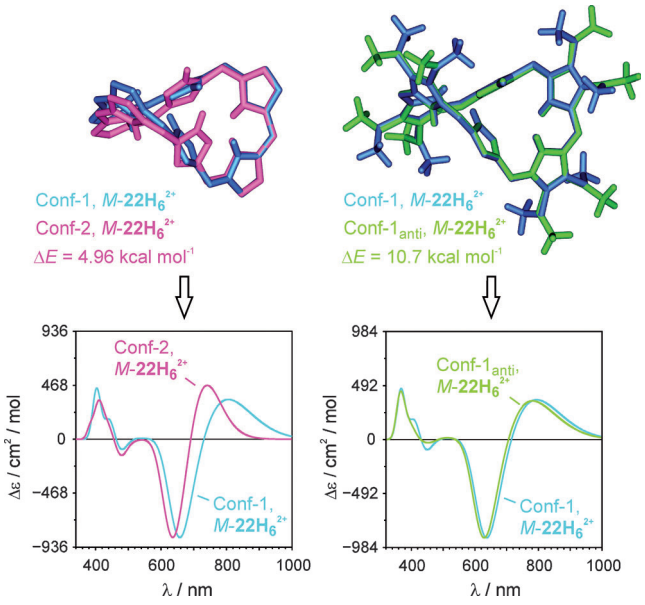

Figure 7. Comparison of conformations of $\mathbf{22H_6}^{2+}$ of the same absolute configuration (here *M*), but with different chromophoric backbones (blue and pink; left), and with completely oppositely orientated ethyl substituents (blue and green, right) and the predicted CD spectra for these conformations.

Even the slight change in the chromophore conformation of $\mathbf{22H_6}^{2+}$ resulted in a significant blueshift (>40 nm) of the first excited states in the CD spectrum predicted for Conf-2 in comparison with the one calculated for the global minimum, represented by Conf-1 (Figure 7, left). This can be explained by the larger difference in the HOMO–LUMO gap of $\Delta E = 1.97$ eV computed for Conf-2 in contrast to $\Delta E = 1.82$ eV simulated for Conf-1 and the fact that the HOMO→LUMO transition accounts for more than 70% of the very first excited state (Conf-1: $\lambda = 852.6$ nm, HOMO→LUMO 76%; Conf-2: $\lambda = 779.7$ nm, HOMO→LUMO 71%). The frontier molecular orbitals also show a strong overlap over the whole macrocyclic framework (Figure 8), Since therefore no significant charge-transfer effects were expected, TDDFT was the method of choice to describe the chiroptical properties of these Siamese-twin porphyrins.

Moreover, due to the larger steric repulsion of the phenyl and ethyl substituents, the enthalpy of formation for Conf-2 was so much increased that this conformer was already out of the energetically relevant range ($\Delta E > 3\ \mathrm{kcal\,mol^{-1}}$ above

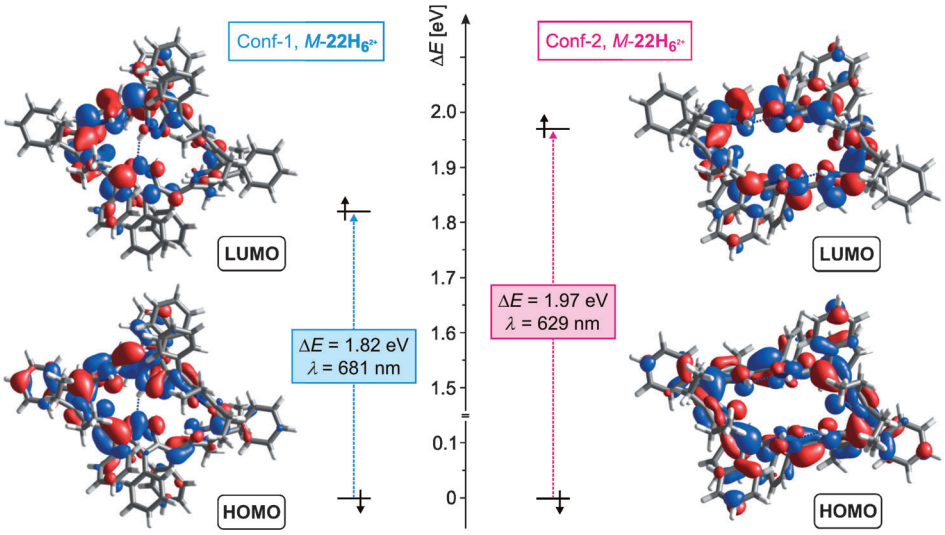

Figure 8. Frontier orbitals obtained from B3LYP/6-31G(d,p) calculations (plotted with an isovalue of 0.0208) showing a strong overlap for both conformations, Conf-1 and Conf-2, and the calculated energies of their HOMO→LUMO transition.

the global minimum). The orientation of the ethyl substituents by contrast had no significant effect on the calculated CD spectrum, as long as the conformers considered possessed the same backbone conformation (Figure 7, right).

Due to this fortunate circumstance, the TD B3LYP/6-31G(d,p) calculation to provide the UV/Vis and CD data needed to be carried out solely for the global minimum conformation of $\mathbf{22H_6}^{2+}$. After a small UV/Vis correction[39] of only 5 nm (see Supporting Information, Figure S18), comparison of the simulated CD curve for *M*-$\mathbf{22H_6}^{2+}$ with the experimental CD spectrum of the more rapidly eluting stereoisomer showed an excellent agreement (peak 1, Figure 9), whereas the CD curve calculated for *P*-$\mathbf{22H_6}^{2+}$ matched well with the one measured for the more slowly eluting enantiomer (peak 2, Figure 9). This permitted not only the unambiguous assignment of the absolute configuration of the two enantiomers of $\mathbf{22H_6}^{2+}$ but also provided additional proof for the existence of the diprotonated species (see Supporting Information, Figures S17 and S19).

Synthesis of the homobimetallic complexes $\mathbf{22Ni_2}$ and $\mathbf{22Cu_2}$: Stirring the deep-green free-base $\mathbf{22H_4}$ with $Cu(OAc)_2{\cdot}H_2O$ in CH_2Cl_2/MeOH 1:1 for 2 h or heating it with $Ni(OAc)_2{\cdot}4H_2O$ in the same solvent system for 24 h resulted in the formation of a blue-green (copper) and burgundy (nickel) complex, respectively (Scheme 4). The relatively low polarity of the isolated materials suggested the formation of neutral complexes. The HR-ESI(+) of the nickel complex indicated the composition $C_{92}H_{80}N_8Ni_2$ (for $[M^+]$), that is, the successful synthesis of the dinickel(II) complex $\mathbf{22Ni_2}$ (see Supporting Information, Figure S11 and S12). In a similar way, the formation of the dicopper complex $\mathbf{22Cu_2}$ was shown by HR-MS ($C_{92}H_{80}N_8Cu_2$). The observation of M^+ parent ions in both cases suggested that the dinickel(II) and dicopper(II) complexes can be readily oxidized to give the corresponding mono-cations, which either are mixed-valence $M^{II}M^{III}$ species or feature non-innocent ligand radicals; this distinction is currently under investigation.

The UV/Vis spectra of the metal complexes displayed hypochromic but otherwise only moderately shifted spectra when compared with the free-base ligand (Figures 1 and 10). Again, the broad bands of near-equal intensity resembled the spectra of the metal complexes of linear oligopyrrolic ligands.[29]

The dicopper complex is paramagnetic.[24] We previously reported the unusual, yet substantial ferromagnetic coupling between the two idealized square-planar d^9 copper centers.[24] The d^8 Ni^{2+} ion in a square-planar coordination sphere is expected to be diamagnetic and, indeed, the ^{1}H NMR spectrum of $\mathbf{22Ni_2}$ showed no signs of any paramagnetic broadening or shifting of the spectrum (see Supporting Information, Figure S13); it resembled the spectrum of $\mathbf{22H_6}^{2+}$·excess TFA (see Supporting Information, Figures S8–S10). The absence of any broadening of the spectra recorded for $\mathbf{22Ni_2}$ was also an indication for the presence of a conformationally rigid structure. Like in the free-base ligand, the diastereotopic splitting of the methylene signals of the β-ethyl groups suggested a non-planar (twisted) conformation and the two distinct methyl signals indicate an overall D_2 symmetry (Figure 11).

Crystal structures of the dinickel(II) and dicopper(II) complexes $\mathbf{22Ni_2}$ and $\mathbf{22Cu_2}$: Crystals of $\mathbf{22Ni_2}$ suitable for X-ray diffraction were obtained by slow solvent evaporation of a saturated solution of $\mathbf{22Ni_2}$ in toluene. The compound crystallized in the non-chiral monoclinic space group *C*2/*c*. Its molecular structure showed the twist along the long axis also seen in the structure of the diprotonated free-base (and the dicopper complex; see below).[24] It thus again crystallized as a racemic mixture of two enantiomeric helimers. The compound exhibited crystallographic two-fold symmetry (D_2 molecular symmetry). The absence of any counterions to each of the nickel(II) centers confirmed the dianionic nature of each metal-binding pocket that was formed by deprotonation of one pyrazole and one pyrrole per binding site. The $\{N_4\}$-coordination sphere of the nickel ions was not entirely planar but slightly twisted towards tetrahedral coordination, with alternating deviations of the nitrogen atoms from the mean plane by ±0.23 Å (angle between the N^{pyr}-Ni-N^{pyr} and the N^{pz}-Ni-N^{pz} planes was 19.2°; Figure 12). This, however, was not enough to cause a fundamental change of metal ion d-orbital splitting from that expected

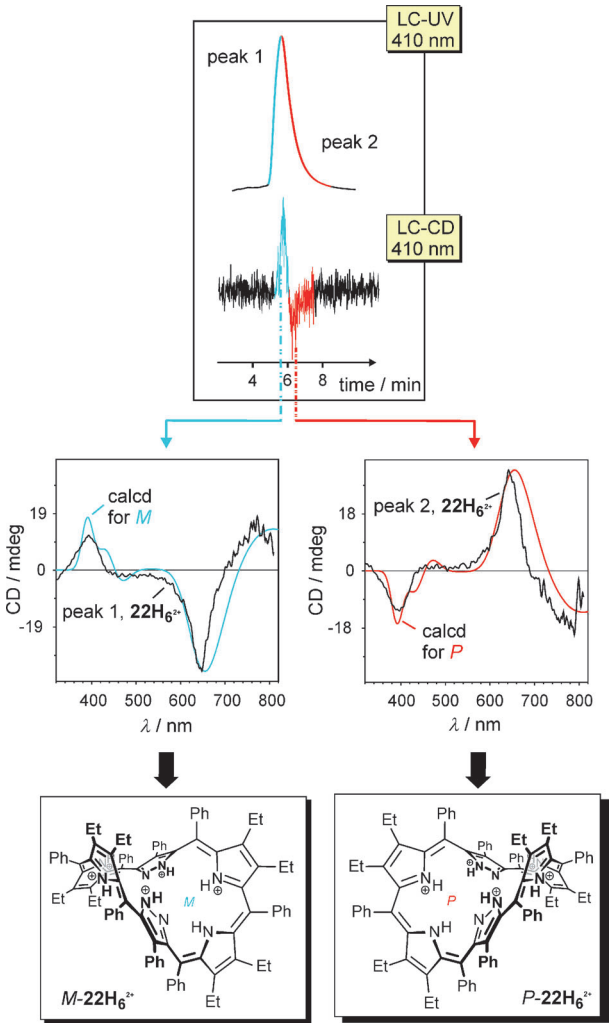

Figure 9. Results of the HPLC separation of a racemic mixture of $\mathbf{22H_6}^{2+}$ on a chiral phase (Chiralpak IA; ambient temperature; ethyl acetate/*n*-hexane (v/v) 30:70, isocratic flow rate: 0.8 mL min^{-1}) and elucidation of the absolute configuration of the two helical enantiomers by comparison of the experimental CD spectra with the calculated CD curves.

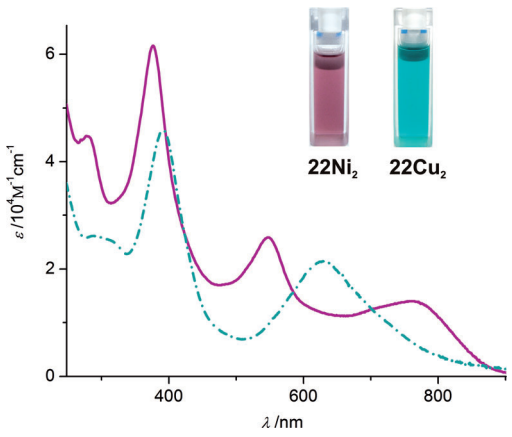

Figure 10. UV/Vis spectra of $\mathbf{22Ni_2}$ (magenta solid trace) and $\mathbf{22Cu_2}$ (blue broken trace) in CH_2Cl_2.

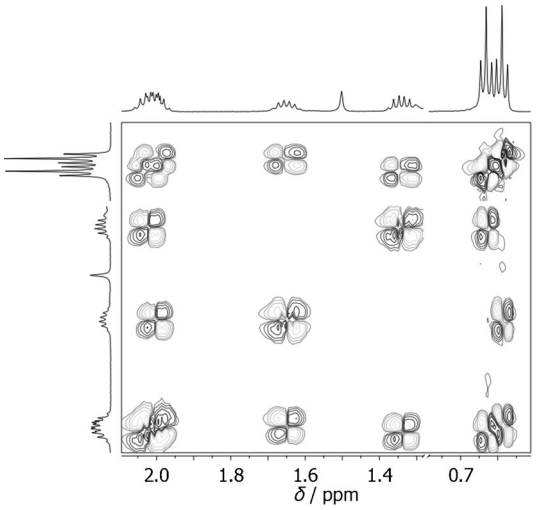

Figure 11. High-field portion (alkyl region) of the $^1H^1H$ COSY spectrum of $\mathbf{22Ni_2}$ (500 MHz, CD_2Cl_2, ambient temperature).

for an idealized planar coordination sphere. The Ni–N bond lengths varied from 1.90 to 1.93 Å with the longer bonds to the pyrazole nitrogen atoms. Owing to the small size of the low-spin nickel(II) ion (0.69 Å),[10c] porphyrins and chlorins also tend to be twisted (ruffled), thus providing short Ni–N bond lengths (1.96 Å were observed for only slightly ruffled nickel(II) porphyrins; strongly ruffled nickel(II) porphyrinoids achieved bond distances as short as 1.89 Å). In contrast to the present case, however, the twist axis in the ruffled nickel(II) porphyrinoids is along the *meso*-$C^{pyr/pyr}$–*meso*-$C^{pyr/pyr}$ axis. Therefore, the ruffling does not distort the coordination sphere of the central metal from planarity. The dicopper complex $\mathbf{22Cu_2}$ also crystallized as a racemic mixture in the space group *C*2/*c*, and also had a similarly twisted conformation as the dinickel complex $\mathbf{22Ni_2}$, although some metric differences were notable (Figure 12). Each copper(II) ion is coordinated in a severely distorted square-planar fashion (the angle between the N^{pyr}-Cu-N^{pyr} and the N^{pz}-Cu-N^{pz} planes is 16.8°). The Cu–N distances are significantly longer than the Ni–N distances in $\mathbf{22Ni_2}$ and range from 1.96 to 2.01 Å, with the longer bonds to the N^{pz} atoms. The differences in the bond lengths between $\mathbf{22Ni_2}$ and $\mathbf{22Cu_2}$ reflect the d^9 electronic structure of the copper(II) with its unpaired electron in the antibonding $d_{x^2-y^2}$ orbital. Overall, each binding pocket is more distorted than in, for instance, [β-octaethyl-*meso*-tetraphenylporphyrinato]-copper(II),[42] highlighting the influence of the twist intrinsic to the ligand. The twist is, with a helimer torsion angle of ±78°, in between that of the nickel complex and the protonated free-base. The Cu···Cu distance of 3.88 Å falls within the range of metal–metal separations found in pyrazolate-bridged binuclear systems.[16]

The overall lengths of the macrocyclic frameworks along their long axes (the $meso^{pyr/pyr}$ to $meso^{pyr/pyr}$ distances) decreased from the protonated macrocycle $\mathbf{22H_6}^{2+}$ (10.72 Å) to $\mathbf{22Cu_2}$ (10.61 Å) to $\mathbf{22Ni_2}$ (10.48 Å), tracking, as expected, with the magnitude of the helimeric twist angles (Figure 12D).

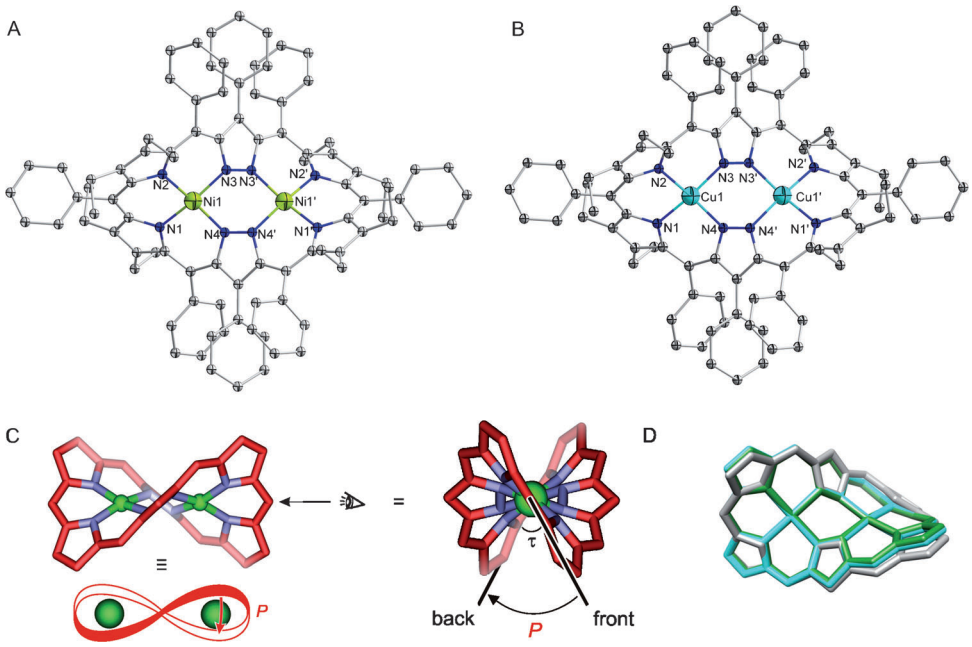

Figure 12. Molecular solid-state structure of A) $\mathbf{22Ni_2}$ (symmetry transformation to generate equivalent atoms (′): $0.5-x$, $0.5+y$, $1.5-z$) and of B) $\mathbf{22Cu_2}$ (symmetry transformation to generate equivalent atoms (′): $1-x$, y, $0.5-z$). C) schematic representation of the *P*-enantiomer, the nomenclature of these helimers and the view along the $meso^{pyr/pyr}$ axis highlighting the torsion angle. D) overlay of the macrocyclic core structures of $\mathbf{22H_6}^{2+}$ (gray), $\mathbf{22Ni_2}$ (olive-green) and $\mathbf{22Cu_2}$ (light blue). All hydrogen atoms and residual solvent molecules were omitted for clarity, as were phenyl and ethyl groups in C and D. Exemplarily only the *P*-helices are shown throughout. The torsion angle τ of ±73° found for $\mathbf{22Ni_2}$ was significantly smaller than that angle observed in the diprotonated free-base $\mathbf{22H_6}^{2+}$. Based on the relatively short N–Ni bond lengths, the stronger twist of the macrocycle seems to be induced by the nickel ions. The Ni···Ni distance of 3.81 Å is similar to metal–metal separations in pyrazolate-bridged binuclear systems (3.3–4.5 Å).[16]

It has been pointed out that the outcomes of metalation experiments of expanded porphyrins are not always predictable.[9c] On account of their flexibility and oxidation sensitivity, this is particularly true for the metalation of hexaphyrins and their *N*-confused congeners.[9c,11] For instance, *meso*-arylhexaphyrin **1** forms a monometallic complex with Ag^{III} and homobimetallic complexes with Ag^{III} and Hg^{II} and a range of $Au^{III}M$ heterobimetallic complexes. The metals are located in plane and each is coordinated by N_2C_2 donor sets.[43] However, the reactions with first-row transition-metals are more complex. For example, treatment of **1** with Cu^{II} or Cu^{I} leads to entirely unanticipated *meso*-position oxidation and dearomatization of the macrocycle or to framework rearrangements to form the C-oxidized version of the doubly *N*-confused hexaphyrin.[44] One other reaction type induced by Pd^{II} includes the formation of Pd–C bonds with concomitant macrocycle dearomatization.[45] The smooth and predictable outcome of the metalation of twin porphyrin $\mathbf{22H_4}$, on the other hand, demonstrates the conformational and chemical stability of this ligand and its potential to serve as scaffold for the targeted formation of bioinspired bimetallic complexes.

Chiral resolution of $\mathbf{22Ni_2}$ and $\mathbf{22Cu_2}$: The solid-state helimeric conformations of the metal complexes $\mathbf{22Ni_2}$ and $\mathbf{22Cu_2}$ were also maintained in solution and, most significantly, the helimeric conformations were persistent and did not racemize (within the timeframe of our observations). We conclude this conformational stability from the straightforward separation of the enantiomeric helimers of both complexes by HPLC on a chiral phase (Figure 13 and the Supporting Information, S14). Excellent resolution was achieved with a 50:50 ratio of ethyl acetate and *n*-hexane on a Chiralpak IB column. For both complexes $\mathbf{22Ni_2}$ and $\mathbf{22Cu_2}$, a clear separation was observed in the LC-UV band. DFT optimization of the global minima of $\mathbf{22Ni_2}$ and $\mathbf{22Cu_2}$ and the UV/Vis and CD spectra calculations were again carried out with the B3LYP functional in combination with the 6-31(d,p) basis set for all elements except for the transition metals, for which the larger 6-311G*[46] basis set was applied. Comparison of the experimental CD spectra with the CD curves calculated for the enantiomers of the two dimetalated complexes revealed an excellent match for the CD spectra of the faster eluting isomers (peak 1, Figure 13) with the one predicted for *M*-$\mathbf{22Ni_2}$ and in the case of $\mathbf{22Cu_2}$ with that of the *P*-enantiomer (the Supporting Information, Figure S14); this led to the unambiguous stereochemical assignment of the helical enantiomers of both dimetalated species.

Conclusion

We have achieved the synthesis of the long sought-after pyrazole-based expanded porphyrin $\mathbf{22H_4}$ and its homobimetallic nickel(II) and copper(II) complexes $\mathbf{22Ni_2}$ and $\mathbf{22Cu_2}$. This macrocycle merges the architecture of two porphyrinoid $\{N_4\}$ coordination sites, but neither of the individual coordination sites, nor the entire macrocycle, showed porphyrinoid aromaticity. The neutral free base was deduced to be conformationally dynamic at the NMR timescale. The protonation behavior of the free base was elucidated by NMR and UV/Vis spectroscopy. These investigations also provided numerous indications for the rigid and twisted conformation of the diprotonated species. The solid-state conformations of the diprotonated free base and the bimetallic complexes were shown to be helimeric. HPLC on a chiral stationary phase allowed us the resolution of $\mathbf{22H_6}^{2+}$, $\mathbf{22Ni_2}$, and

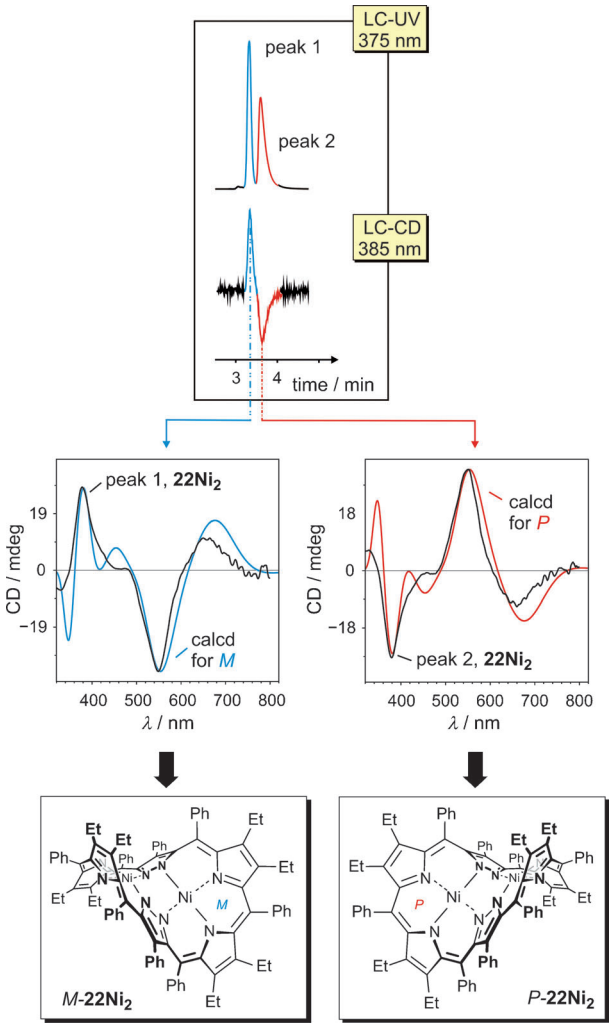

Figure 13. Results of the HPLC resolution of a racemic mixture of **22Ni$_2$** on a chiral phase (Chiralpak IB; ambient temperature; ethyl acetate/*n*-hexane (v/v) 50:50, isocratic flow rate: 1.5 mL min^{-1}) and stereochemical assignment of the two enantiomers by comparison of their experimental CD spectra with the quantum-chemically computed ones.

22Cu$_2$ into their enantiomers and the unambiguous determination of their absolute configurations by a combination of experimental and quantum-chemical ECD investigations. Thus, the twin porphyrin and its metal complexes provide another, and new, example of the class of porphyrins with persistent chirality. Moreover, their metal-binding pocket permits the formation of bimetallic complexes in which the metals are close enough to interact with each other and potentially also with a range of bridging axial ligands. Thus, these macrocycles provide a new scaffold for the study of bimetallic multi-electron processes or the biomimetic activation of small molecules, aspects we are currently investigating.

Acknowledgements

Financial support from the Fonds der Chemischen Industrie and the DAAD (fellowships to L.K.B) as well as the NSF (CHE-0517782 and 1058846, both to C.B.) is gratefully acknowledged.

[1] V. J. Bauer, D. L. J. Clive, D. Dolphin, J. B. Paine, F. L. Harris, M. M. King, J. Loder, S. W. C. Wang, R. B. Woodward, *J. Am. Chem. Soc.* **1983**, *105*, 6429–6436.
[2] a) P. A. Gale, S. E. Garcia-Garrido, J. Garric, *Chem. Soc. Rev.* **2008**, *37*, 151–190; b) J. L. Sessler, S. Camiolo, P. A. Gale, *Coord. Chem. Rev.* **2003**, *240*, 17–55.
[3] a) M. Stepień, L. Latos-Grazyński, *Top. Heterocyc. Chem.* **2009**, *19*, 83–153; b) A. Osuka, S. Saito, *Chem. Commun.* **2011**, *47*, 4330–4339.
[4] Z. S. Yoon, A. Osuka, D. Kim, *Nat. Chem.* **2009**, *1*, 113–122.
[5] J. L. Sessler, A. E. Vivian, D. Seidel, A. K. Burrell, M. Hoehner, T. D. Mody, A. Gebauer, S. J. Weghorn, V. Lynch, *Coord. Chem. Rev.* **2001**, *216–217*, 411–434.
[6] a) J. L. Sessler, N. A. Tvermoes, J. Davis, P. J. Anzenbacher, K. Jursíková, W. Sato, D. Seidel, V. Lynch, C. B. Black, A. Try, B. Andrioletti, G. Hemmi, T. D. Mody, D. J. Magda, V. Kral, *Pure Appl. Chem.* **1999**, *71*, 2009–2018; b) J. L. Sessler, G. Hemmi, T. D. Mody, T. Murai, A. Burrell, S. W. Young, *Acc. Chem. Res.* **1994**, *27*, 43–50; c) T. D. Mody, J. L. Sessler, *J. Porphyrins Phthalocyanines* **2001**, *5*, 134–142; d) D. J. Magda, Z. Wang, N. Gerasimchuk, P. J. Anzenbacher, J. L. Sessler, *Pure Appl. Chem.* **2004**, *76*, 365–374.
[7] a) J. L. Sessler, T. D. Mody, G. W. Hemmi, V. Lynch, S. W. Young, R. A. Miller, *J. Am. Chem. Soc.* **1993**, *115*, 10368–10369; b) S. W. Young, F. Qing, A. Harriman, J. L. Sessler, W. C. Dow, T. D. Mody, G. W. Hemmi, Y. Hao, R. A. Miller, *Proc. Natl. Acad. Sci. USA* **1996**, *93*, 6610–6615.
[8] J. M. Lim, Z. S. Yoon, J.-Y. Shin, K. S. Kim, M.-C. Yoon, D. Kim, *Chem. Commun.* **2009**, 261–273.
[9] a) R. Misra, T. K. Chandrashekar, *Acc. Chem. Res.* **2008**, *41*, 265–279; b) J. L. Sessler, A. Gebauer, S. J. Weghorn in *The Porphyrin Handbook, Vol. 2* (Eds.: K. M. Kadish, K. M. Smith, R. Guilard), Academic Press, San Diego, USA, **2000**, pp. 55–124; c) S. Saito, A. Osuka, *Angew. Chem.* **2011**, *123*, 4432–4464; *Angew. Chem. Int. Ed.* **2011**, *50*, 4342–4373; d) M. Stępień, N. Sprutta, L. Latos-Grażyński, *Angew. Chem.* **2011**, *123*, 4376–4430; *Angew. Chem. Int. Ed.* **2011**, *50*, 4288–4340; e) A. Jasat, D. Dolphin, *Chem. Rev.* **1997**, *97*, 2267–2340; f) J. L. Sessler, S. Weghorn, *Expanded, Contracted & Isomeric Porphyrins*, Pergamon, New York, **1997**; g) T. K. Chandrashekar, S. Venkatraman, *Acc. Chem. Res.* **2003**, *36*, 676–691.
[10] a) L.-A. Fendt, H. Fang, M. E. Ploska-Brzezinska, S. Zhang, F. Cheng, C. Braun, L. Echegoyen, F. Diederich, *Eur. J. Org. Chem.* **2007**, 4659–4673; b) Y. Nakamura, N. Aratani, H. Shinokubo, A. Takagi, T. Kawai, T. Matsumoto, Z. S. Yoon, D. Y. Kim, T. K. Ahn, D. Kim, A. Muranaka, N. Kobayashi, A. Osuka, *J. Am. Chem. Soc.* **2006**, *128*, 4119–4127; c) L. Arnold, S. R. Puniredd, C. v. Malotki, W. Pisula, N. Koshino, H. Higashimura, M. Baumgarten, M. Wagner, K. Müllen, *J. Porphyrins Phthalocyanines* **2012**, *16*, 564–575.
[11] M. Toganoh, H. Furuta, *Chem. Commun.* **2012**, *48*, 937–954.
[12] a) P. J. Chmielewski, *Angew. Chem.* **2010**, *122*, 1399–1401; *Angew. Chem. Int. Ed.* **2010**, *49*, 1359–1361; b) M. Toganoh, H. Furuta, in *Handbook of Porphyrin Science Vol. 2* (Eds.: K. M. Kadish, K. M. Smith, R. Guilard), World Scientific, Singapore, **2010**, p. 295; c) J. W. Buchler, in *Porphyrins, Vol. 1* (Ed.: D. Dolphin), Academic Press, New York, **1978**, pp. 389–483; d) J. L. Sessler, E. Tomat, *Acc. Chem. Res.* **2007**, *40*, 371–379.
[13] M. G. P. M. S. Neves, R. M. Martins, A. C. Tome, A. J. D. Silvestre, A. M. S. Silva, V. Felix, J. A. S. Cavaleiro, M. G. B. Drew, *Chem. Commun.* **1999**, 385–386.
[14] a) C. Bucher, D. Seidel, V. Lynch, J. L. Sessler, *Chem. Commun.* **2002**, 328–329; b) J. L. Sessler, D. Seidel, V. Lynch, *J. Am. Chem. Soc.* **1999**, *121*, 11257–11258.

[15] E. Vogel, M. Bröring, J. Fink, D. Rosen, H. Schmickler, J. Lex, K. W. K. Chan, Y.-D. Wu, D. A. Plattner, M. Nendel, K. N. Houk, *Angew. Chem.* **1995**, *107*, 2705–2709; *Angew. Chem. Int. Ed. Engl.* **1995**, *34*, 2511–2514.

[16] J. Klingele, S. Dechert, F. Meyer, *Coord. Chem. Rev.* **2009**, *253*, 2698–2741.

[17] a) F. Meyer, *Eur. J. Inorg. Chem.* **2006**, 3789–3800; b) A. Prokofieva, A. I. Prikhod'ko, E. A. Enyedy, E. Farkas, W. Maringgele, S. Demeshko, S. Dechert, F. Meyer, *Inorg. Chem.* **2007**, *46*, 4298–4307; c) H. Müller, B. Bauer-Siebenlist, E. Csapo, S. Dechert, E. Farkas, F. Meyer, *Inorg. Chem.* **2008**, *47*, 5278–5292; d) T. Graef, J. Galezowska, S. Dechert, F. Meyer, *Eur. J. Inorg. Chem.* **2011**, 4161–4167; e) B. Burger, S. Dechert, C. Große, S. Demeshko, F. Meyer, *Chem. Commun.* **2011**, *47*, 10428–10430.

[18] a) F. Meyer, K. Heinze, B. Nuber, L. Zsolnai, *J. Chem. Soc. Dalton Trans.* **1998**, 207–213; b) F. Meyer, P. Rutsch, *Chem. Commun.* **1998**, 1037–1038; c) J. Ackermann, F. Meyer, E. Kaifer, H. Pritzkow, *Chem. Eur. J.* **2002**, *8*, 247–258; d) S. Buchler, F. Meyer, E. Kaifer, H. Pritzkow, *Inorg. Chim. Acta* **2002**, *337*, 371–386.

[19] a) J. Akhigbe, J. Haskoor, M. Zeller, C. Brückner, *Chem. Commun.* **2011**, *47*, 8599–8601; b) J. Akhigbe, G. Peters, M. Zeller, C. Brückner, *Org. Biomol. Chem.* **2011**, *9*, 2306–2313.

[20] a) A. M. Shulga, I. M. Biteva, I. F. Gurinovich, L. A. Grubina, G. P. Gurinovich, *Biofizika* **1977**, *22*, 771–776; b) M. J. Crossley, L. G. King, *J. Chem. Soc. Chem. Commun.* **1984**, 920–922; c) M. Gouterman, R. J. Hall, G. E. Khalil, P. C. Martin, E. G. Shankland, R. L. Cerny, *J. Am. Chem. Soc.* **1989**, *111*, 3702–3707; d) J. Ogikubo, C. Brückner, *Org. Lett.* **2011**, *13*, 2380–2383; e) S. V. Dudkin, E. A. Makarova, T. Fukuda, N. Kobayashi, E. A. Lukyanets, *Tetrahedron Lett.* **2011**, *52*, 2994–2996; f) J. Ogikubo, E. Meehan, J. T. Engle, C. Ziegler, C. Brückner, *J. Org. Chem.* **2012**, *77*, 6199–6207.

[21] a) M. Nicolau, B. Cabezón, T. Torres, *Coord. Chem. Rev.* **1999**, *190–192*, 231–243; b) J. Mack, N. Kobayashi, *Chem. Rev.* **2011**, *111*, 281–321.

[22] a) T. D. Lash, A. M. Young, A. L. Von Ruden, G. M. Ferrence, *Chem. Commun.* **2008**, 6309–6311; b) A. M. Young, A. L. Von Ruden, T. D. Lash, *Org. Biomol. Chem.* **2011**, *9*, 6293–6305; c) See also their review in: T. D. Lash in *Handbook of Porphyrin Science Vol. 16* (Eds.: K. M. Kadish, K. M. Smith, R. Guilard), World Scientific, Singapore, **2012**, pp. 231–241.

[23] a) S. Katsiaouni, S. Dechert, C. Brückner, F. Meyer, *Chem. Commun.* **2007**, 951–953; b) S. Katsiaouni, S. Dechert, R. P. Brinas, C. Brückner, F. Meyer, *Chem. Eur. J.* **2008**, *14*, 4823–4835.

[24] L. K. Frensch, K. Pröpper, M. John, S. Demeshko, C. Brückner, F. Meyer, *Angew. Chem.* **2011**, *123*, 1456–1460; *Angew. Chem. Int. Ed.* **2011**, *50*, 1420–1424.

[25] a) E. J. Lind, M.Sc. Thesis, Michigan State University, East Lansing, MI, USA, **1984**; b) E. J. Lind, Ph.D. Thesis, Michigan State University, East Lansing, MI, USA, **1987**. The target macrocycle was referred to as octaaza-[1.5.1.5]platyrin. This work was part of the efforts of the group of E. LeGoff on the synthesis of vinylogous expanded porphyrins, see ref. [9], pp. 201–215.

[26] A. Sachse, L. Penkova, G. Noel, S. Dechert, O. A. Varzatskii, I. O. Fritsky, F. Meyer, *Synthesis* **2008**, 800–806.

[27] D. Dolphin, *J. Heterocycl. Chem.* **1970**, *7*, 275–283.

[28] M. Gouterman, in *The Porphyrins, Vol. 3* (Eds.: D. Dolphin), Academic Press, New York, **1978**, pp. 1–165.

[29] H. Falk, *The Chemistry of Linear Oligopyrroles and Bile Pigments*, Springer, New York, **1989**.

[30] A. Werner, M. Michels, L. Zander, J. Lex, E. Vogel, *Angew. Chem.* **1999**, *111*, 3866–3870; *Angew. Chem. Int. Ed.* **1999**, *38*, 3650–3653.

[31] S. Berger, S. Braun, H.-O. Kalinowski, *NMR Spectroscopy of the Non-metallic Elements*, Wiley, New York, **1996**.

[32] a) F. Neese, ORCA, An ab initio density functional and semiempirical program package, University of Bonn (Germany), **2007**; b) F. Neese, The ORCA program system, *WIREs Comput. Mol. Sci.* **2012**, *2*, 73–78.

[33] S. Shimizu, N. Aratani, A. Osuka, *Chem. Eur. J.* **2006**, *12*, 4909–4918.

[34] C. J. Medforth, M. O. Senge, K. M. Smith, L. D. Sparks, J. A. Shelnutt, *J. Am. Chem. Soc.* **1992**, *114*, 9859–9869.

[35] S. Saito, A. Osuka, *Chem. Eur. J.* **2006**, *12*, 9095–9102.

[36] C. Brückner, D. C. G. Götz, S. P. Fox, C. Ryppa, J. R. McCarthy, T. Bruhn, J. Akhigbe, S. Banerjee, P. Daddario, H. W. Daniell, M. Zeler, R. W. Boyle, G. Bringmann, *J. Am. Chem. Soc.* **2011**, *133*, 8740–8752.

[37] a) G. Bringmann, D. C. G. Götz, T. Bruhn, in *Comprehensive Chiroptical Spectroscopy, Vol. 2* (Eds.: N. Berova, P. L. Polavarapu, K. Nakanishi, R. W. Woody), Wiley, Hoboken, **2012**, pp. 355–420; b) G. Bringmann, T. A. M. Gulder, M. Reichert, T. Gulder, *Chirality* **2008**, *20*, 628–642.

[38] G. Bringmann, T. Bruhn, K. Maksimenka, Y. Hemberger, *Eur. J. Org. Chem.* **2009**, 2717–2727.

[39] D. C. G. Götz, T. Bruhn, M. O. Senge, G. Bringmann, *J. Org. Chem.* **2009**, *74*, 8005–8020.

[40] Gaussian 09, Revision B.01, M. J. Frisch, G. W. Trucks, H. B. Schlegel, G. E. Scuseria, M. A. Robb, J. R. Cheeseman, G. Scalmani, V. Barone, B. Mennucci, G. A. Petersson, H. Nakatsuji, M. Caricato, X. Li, H. P. Hratchian, A. F. Izmaylov, J. Bloino, G. Zheng, J. L. Sonnenberg, M. Hada, M. Ehara, K. Toyota, R. Fukuda, J. Hasegawa, M. Ishida, T. Nakajima, Y. Honda, O. Kitao, H. Nakai, T. J. A. Vreven, J. Montgomery, J. E. Peralta, F. Ogliaro, M. Bearpark, J. J. Heyd, E. Brothers, K. N. Kudin, V. N. Staroverov, T. Keith, R. Kobayashi, J. Normand, K. Raghavachari, A. Rendell, J. C. Burant, S. S. Iyengar, J. Tomasi, M. Cossi, N. Rega, J. M. Millam, M. Klene, J. E. Knox, J. B. Cross, V. Bakken, C. Adamo, J. Jaramillo, R. Gomperts, R. E. Stratmann, O. Yazyev, A. J. Austin, R. Cammi, C. Pomelli, J. W. Ochterski, R. L. Martin, K. Morokuma, V. G. Zakrzewski, G. A. Voth, P. Salvador, J. J. Dannenberg, S. Dapprich, A. D. Daniels, O. Farkas, J. B. Foresman, J. V. Ortiz, J. Cioslowski, D. J. Fox, Wallingford CT, **2010**.

[41] a) P. C. Hariharan, J. A. Pople, *Theor. Chim. Acta* **1973**, *28*, 213–222; b) W. J. Hehre, R. Ditchfield, J. A. Pople, *J. Chem. Phys.* **1972**, *56*, 2257–2261; c) C. Lee, W. Yang, R. G. Parr, *Phys. Rev. B* **1988**, *37*, 785–789; d) A. D. Becke, *J. Chem. Phys.* **1993**, *98*, 5648–5652.

[42] L. D. Sparks, C. J. Medforth, M. S. Park, J. R. Chamberlain, M. R. Ondrias, M. O. Senge, K. M. Smith, J. A. Shelnutt, *J. Am. Chem. Soc.* **1993**, *115*, 581–592.

[43] a) S. Mori, A. Osuka, *Inorg. Chem.* **2008**, *47*, 3937–3939; b) A. Mori, S. Shimizu, J.-Y. Shin, A. Osuka, *Inorg. Chem.* **2007**, *46*, 4374–4376.

[44] a) S. Shimizu, V. G. Anand, R. Taniguchi, K. Furukawa, T. Kato, T. Yokoyama, A. Osuka, *J. Am. Chem. Soc.* **2004**, *126*, 12280–12281; b) M. Suzuki, M.-C. Yoon, D. Y. Kim, J. H. Kwon, H. Furuta, D. Kim, A. Osuka, *Chem. Eur. J.* **2006**, *12*, 1754–1759.

[45] S. Mori, S. Shimizu, R. Taniguchi, A. Osuka, *Inorg. Chem.* **2005**, *44*, 4127–4129.

[46] a) R. Krishnan, J. S. Binkley, R. Seeger, J. A. Pople, *J. Chem. Phys.* **1980**, *72*, 650–654; b) K. Raghavachari, G. W. Trucks, *J. Chem. Phys.* **1989**, *91*, 2457–2460.

Received: December 3, 2012
Published online: ■■ ■■, 2013

Expanded Porphyrins

L. K. Blusch, Y. Hemberger, K. Pröpper, B. Dittrich, F. Witterauf, M. John, G. Bringmann, C. Brückner,* F. Meyer** .... ■■■■–■■■■

VIP **Siamese-Twin Porphyrin: A Pyrazole-Based Expanded Porphyrin of Persistent Helical Conformation**

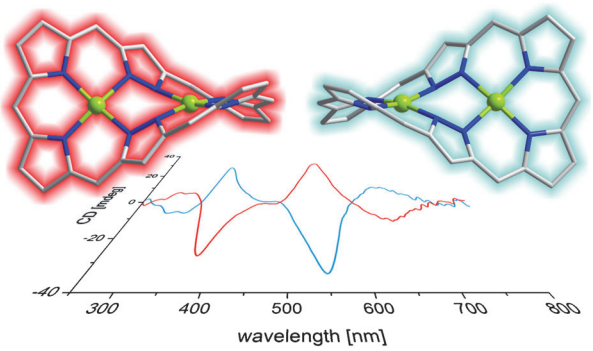

The chiral twist: The first pyrazole-based expanded porphyrin is highly twisted, which implies helical chirality. Besides the separation of the helical enantiomers of the free base, a thorough understanding of the origin of the twist and its pH dependency was obtained (see figure). First bimetallic nickel and copper complexes were synthesized, in which each metal is embedded in a porphyrin-like $\{N_4\}$ pocket. The complexes were fully characterized, including the resolution of helimers.

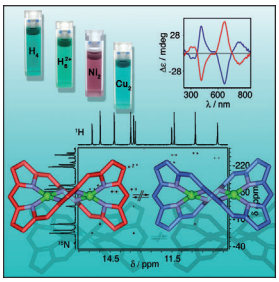

VIP **Expanded porphyrins**

The synthesis of the long sought-after pyrazole-based expanded porphyrin and its homobimetallic nickel(II) and copper(II) complexes is described in the Full Paper by G. Bringmann, C. Brückner, F. Meyer et al. on page ■■ ff. Spectroscopic evidence as well as structural parameters of this hexaphyrin analogue (named the Siamese-twin porphyrin) proved it to be non-aromatic, though each half of the molecule is fully conjugated. In the complexes, each metal ion is coordinated in a square-planar fashion by a dianionic, porphyrin-like $\{N_4\}$ binding pocket. The conformations of the diprotonated macrocycle and its metal complexes are all strongly twisted. The persistent helical twist permitted resolution of the enantiomeric helimers by HPLC on a chiral phase.